Improving the Structural Stability of TEMPO-Oxidized Cellulose Nanofibril Hydrogels through Chitin Nanofibril Reinforcement and Hydrothermal Treatment

Seung-Woo Cho,[a] Ju-Won Jin,[a] Dong-Suk Jeon,[a] Ramakrishna Dadigala,[b] Song-Yi Han,[b] Gu-Joong Kwon,[b] Rajkumar Bandi,[b] Sang-Jin Chun,[c] Jaegyoung Gwon,[d] and Seung-Hwan Lee [a,b,*]

Hydrogels based on TEMPO-oxidized cellulose nanofibrils (TOCNF) are attractive sustainable materials but often suffer from poor structural stability and weak mechanical strength. In this study, surface-deacetylated chitin nanofibrils (ChNF) were incorporated to reinforce TOCNF hydrogels, and the effect of hydrothermal treatment on network structure and properties was investigated. Hydrogels were prepared at solid contents of 1.25 to 2.00 wt% by mixing dilute TOCNF and ChNF suspensions followed by centrifugation and hydrothermal treatment. Compared with TOCNF alone, TOCNF/ChNF hydrogels exhibited improved shape stability, higher viscosity, and enhanced shear-thinning behavior. Hydrothermally treated TOCNF/ChNF hydrogels maintained elastic behavior up to 74.6% strain, compared with 26.3% strain for non-treated TOCNF/ChNF hydrogels. The compressive strength increased markedly, reaching 36 kPa at 1.75 wt%, whereas TOCNF hydrogels showed only ~5 kPa. FTIR and XPS analyses indicated redistribution of intermolecular interactions after hydrothermal treatment without definitive evidence of covalent bond formation. SEM observations further revealed the formation of a more interconnected and densified porous network after hydrothermal treatment. Overall, ChNF reinforcement combined with hydrothermal treatment effectively improved the structural stability and mechanical performance of TOCNF hydrogels.

DOI: 10.15376/biores.21.3.6016-6035

Keywords: TEMPO-oxidized cellulose nanofibrils (TOCNFs); Surface-deacetylated chitin nanofibrils; Nanocomposite hydrogels; Physical crosslinking; Structural and mechanical stability

Contact information: a: Department of Forest Biomaterials Engineering, College of Forest and Environmental Sciences, Kangwon National University, Chuncheon, 24341, Republic of Korea; b: Institute of Forest Science, Kangwon National University, Chuncheon, 24341, Republic of Korea; c: National Institute of Forest Science, Seoul 02455, Republic of Korea; d: Department of Wood Science and Technology, Jeonbuk National University, Jeonju, 54896, Republic of Korea
** Corresponding author: lshyhk@kangwon.ac.kr*

INTRODUCTION

Hydrogels are three-dimensional polymer networks capable of absorbing large amounts of water while maintaining structural integrity (Ahmed 2015; Sharma *et al.* 2024). Because of their high-water content, soft mechanical characteristics, and tunable physical properties, hydrogels have attracted considerable attention for applications in tissue engineering, drug delivery, wound dressings, and environmental remediation (Correa *et al.* 2021). In recent years, increasing interest has been directed toward hydrogels derived from

renewable biopolymers as sustainable alternatives to synthetic polymer systems (Tariq *et al.* 2023; Mehvari *et al.* 2024).

Among natural biopolymers, cellulose nanofibrils (CNFs) have emerged as promising building blocks for hydrogel fabrication due to their high aspect ratio, large surface area, and excellent mechanical properties (Du and Feng 2023) (Alghonaim *et al.* 2024). In particular, 2,2,6,6-tetramethylpiperidine-1-oxyl(TEMPO)-oxidized cellulose nanofibrils (TOCNFs) contain abundant surface carboxyl groups that provide strong electrostatic repulsion and good dispersibility in water, enabling the formation of highly entangled nanofibrillar networks (Nikolits *et al.* 2023; Tang *et al.* 2024). These features make TOCNF-based hydrogels attractive for various biomedical and environmental applications (Lan *et al.* 2021; Shi *et al.* 2025). However, hydrogels prepared solely from TOCNF often exhibit limited structural stability and relatively low mechanical strength, which restrict their practical use (Chinga-Carrasco 2018; Altynov *et al.* 2025).

Several strategies have been explored to improve the stability and mechanical properties of nanocellulose hydrogels (De France *et al.* 2017; Zafar *et al.* 2022). These include increasing fibril concentration, introducing physical crosslinking through ionic interactions or hydrogen bonding, and incorporating secondary polymers to reinforce the fibrillar network (Liang *et al.* 2020). Among these approaches, combining nanocellulose with another nanoscale biopolymer is particularly promising, as the interaction between different fibrillar components can enhance network formation while maintaining the renewable and biodegradable nature of the materials.

Chitin is the second most abundant natural polysaccharide after cellulose and possesses a highly crystalline nanofibrillar structure with excellent mechanical properties (Shen *et al.* 2015; Jin *et al.* 2021). Chitin nanofibrils (ChNF) have attracted attention as reinforcing elements in bio-based materials because of their high stiffness and fibrous morphology (Tsutsumi *et al.* 2014; Jin *et al.* 2021; Saied *et al.* 2023). When partially deacetylated, the surface of ChNF contains amino groups that can interact with negatively charged polysaccharides, such as TOCNF, through electrostatic attraction and hydrogen bonding. Such interactions may promote the formation of a more stable fibrillar network in hydrogel systems. Previous studies have reported hydrogels based on TOCNF–ChNF mixtures (Zhang *et al.* 2019; Noda *et al.* 2022). However, these studies have primarily focused on material preparation, and a systematic understanding of how ChNF incorporation influences structural stability and mechanical behavior remains limited.

In addition to compositional modification, post-treatment strategies such as hydrothermal treatment can influence the structural organization of polysaccharide-based hydrogels (Suenaga *et al.* 2019; Wasupalli *et al.* 2023). Hydrothermal conditions have been reported to promote fibrillar rearrangement, network densification, and enhanced intermolecular interactions, leading to improved mechanical stability in CNF and related biopolymer systems (Suenaga *et al.* 2018; Nata *et al.* 2012). Despite this, the role of hydrothermal treatment in regulating the structure–property relationships of TOCNF–ChNF hydrogels has not been clearly established.

Therefore, the key knowledge gap lies in understanding how the combination of ChNF incorporation and hydrothermal treatment influences the network structure, intermolecular interactions, and resulting mechanical performance of TOCNF-based hydrogels.

This study (i) investigated the effect of ChNF incorporation on the formation and stability of TOCNF-based hydrogels, and (ii) elucidated how hydrothermal treatment modifies the fibrillar network structure and enhances mechanical properties. Hydrogels

were prepared by combining TOCNF and ChNF at different concentrations, followed by hydrothermal treatment under controlled conditions. The resulting materials were systematically characterized using rheological measurements, compression testing, scanning electron microscopy (SEM), Fourier transform infrared spectroscopy (FTIR), X-ray photoelectron spectroscopy (XPS), and thermogravimetric analysis (TGA). The results can provide insight into the structure–property relationships governing the stability and performance of TOCNF/ChNF hydrogel systems.

EXPERIMENTAL

Materials

Hardwood kraft pulp obtained from Moorim P&P Co., Ltd. (Ulsan, Republic of Korea) was used as the raw material for preparing TOCNF. Other reagents, including TEMPO, sodium bromide, 30% sodium hypochlorite solution, ethyl alcohol 99.5%, 50% NaOH solution, and hydrochloric acid, were purchased from Daejung Chemicals & Metals Co., Ltd. (Siheung, Republic of Korea). Chitin Nanofibrils (ChNF) (degree of deacetylation greater than 50%, fiber width of 1 to 20 nm) was obtained from ANPOLY Inc. (Pohang, Republic of Korea).

TOCNF Preparation

A 1 g sample of hardwood kraft pulp was combined with 99 g of distilled water, 16 mg of TEMPO, and 100 mg of NaBr. The mixture was stirred until the TEMPO was completely dissolved. To initiate the reaction, 3.5 mL of a 12% NaClO solution was added. During the reaction, the pH of the mixture was maintained at 10 by the addition of 0.5 M NaOH. The reaction was continued for approximately 5 h, or until the pH no longer decreased. To terminate the reaction, 5 mL of ethanol was added, and the pH was then adjusted to 7.5 using 0.1 M HCl. The resulting sample was washed with excess distilled water *via* vacuum filtration. Finally, the product was homogenized at 20,000 psi (138 MPa) using a high-pressure homogenizer (MN400BF, Micronox, Seoul, Republic of Korea).

Determination of Amine and Carboxyl Group Contents

The primary amine ($-NH_2$) content of ChNF and the carboxyl group content of TOCNF were determined by conductometric titration following the method reported by (Zhang *et al.* 2019) (details in Supporting Information). The TOCNF showed a carboxyl content of 0.69 ± 0.03 mmol/g, while the amine content of ChNF was 3.43 ± 0.04 mmol/g.

Preparation of TOCNF/ChNF Hydrogels

A 0.1 wt% TOCNF suspension and a 0.1 wt% ChNF suspension were prepared separately and then mixed at a 1:1 volume ratio under stirring at 300 rpm. The ChNF suspension was added dropwise to the TOCNF suspension during mixing. The resulting mixture was centrifuged at 11,000, 13,000, 15,000, and 17,000 rpm for 10 min to obtain hydrogels with solid contents of 1.25, 1.50, 1.75, and 2.00 wt%, respectively. For hydrothermal treatment, the as-prepared hydrogels were sealed in a Teflon lined stainless-steel autoclave and heated at 110, 130, or 150 °C for 2 h. For clarity, samples are denoted as TOCNF-H (hydrothermally treated TOCNF), TOCNF/ChNF (non-treated mixture), and TOCNF/ChNF-H (hydrothermally treated composite).

Morphological Observation

For morphological analysis, 0.001 wt% suspensions of TOCNF and ChNF were prepared by sonicating them for 60 s using a sonicator (VCX103PB, Sonics and Materials, Inc., Newtown, USA). The resulting dispersions were then vacuum-filtered using a polytetrafluoroethylene membrane filter with a pore size of 0.2 µm (Toyo Roshi Kaisha, Ltd., Tokyo, Japan). To prepare the samples for imaging, the residual material on the filter was treated with tert-butyl alcohol three times, for 20 min each, to perform a solvent exchange where water was replaced with tert-butyl alcohol. The samples were then frozen at −20 °C for 5 h before being freeze-dried for 5 h at −50 °C. Subsequently, the dried samples were mounted on aluminum stubs and coated with a 2-nm-thick layer of iridium using a high-vacuum sputter coater (EM ACE600, Leica Microsystems, Ltd., Wetzlar, Germany). The prepared samples were then observed using a field-emission scanning electron microscope (FE-SEM) (S-4800, Hitachi, Tokyo, Japan). The diameters of the TOCNF and ChNF fibers were determined by measuring over 100 fibers from the acquired SEM images using Image-J software (Version 1.52, University of Wisconsin, Madison, WI, USA). The average values were then calculated. The morphology of TOCNF/ChNF and TOCNF/ChNF-H hydrogels was also analyzed using FE-SEM. For this purpose, the hydrogels were freeze-dried, mounted on aluminum stubs, sputter-coated with iridium, and observed under the same conditions described above.

Viscosity and Rheology

The viscosity and rheology of the hydrogels was measured using a MCR 702e Multidrive rheometer (Anton Paar, Graz, Austria). All measurements were conducted using bottom plate 50 mm and a 25 mm top plate with 1 mm gap. The temperature was set to 25 °C for all experiments. Viscosity measurements were obtained in the shear rate range of 0.01 to 1000 s^{-1}. Amplitude sweep measurements for hydrogel's storage modulus and loss modulus were obtained in the shear strain range of 0.01 to 100%.

Mechanical Property of Hydrogels

The compressive strength of both hydrogels was evaluated using an MCR 702e Multidrive rheometer (Anton Paar, Graz, Austria). Measurements were performed at 25 °C with a 50 mm bottom plate and a 25 mm top plate. The height of all hydrogel samples was standardized to 20 mm to ensure consistency.

X-Ray Photoelectron Spectroscopy

The surface chemical properties of TOCNF and TOCNF/ChNF were analyzed using X-ray photoelectron spectroscopy (XPS, K alpha+, Thermo Fisher Scientific, Waltham, MA, USA). Hydrogels were freeze-dried and pressed into films prior to analysis.

Fourier-Transform Infrared Spectroscopy

The samples were analyzed using Fourier-transform infrared (FT-IR, Nicolet iS50, Thermo Fisher Scientific, Waltham, MA, USA) spectroscopy in attenuated total reflection (ATR) mode. In total, 64 scans were performed for each sample in the range of 4,000 to 800 cm^{-1}, with a resolution of 4 cm^{-1}. Hydrogels were freeze-dried and pressed into films prior to analysis.

Thermal Properties

The thermal decomposition characteristics were analyzed using a thermo-gravimetric analyzer (SDT Q600, TA Instruments, New Castle, DE, USA). Samples were analyzed in the temperature range of 25 to 500 °C at a constant heating rate of 10 °C/min, with a nitrogen gas flow rate of 100 mL/min. Hydrogels were freeze-dried and pressed into films prior to analysis.

Statistical Analysis

All experiments were conducted in triplicate, and data are reported as mean ± standard deviation. Error bars shown in the figures correspond to the standard deviation obtained from three independent measurements.

RESULTS AND DISCUSSION

Morphological Properties of TOCNF and ChNF

Figure 1 displays the FE-SEM images of TOCNF and ChNF, both exhibiting interconnected nanofibrillar network structures. The TOCNF nanofibrils appeared relatively uniform, with an average diameter of 16.85 ± 4.62 nm, forming a dense and entangled web-like morphology. In contrast, ChNF nanofibrils were slightly thicker, with an average diameter of 25.86 ± 5.76 nm, and displayed a comparatively looser network arrangement. The differences in fibril diameter and packing density are attributed to the distinct chemical structures of cellulose and chitin, which influence their fibrillation behavior and surface interactions (Jin and Spontak 2023).

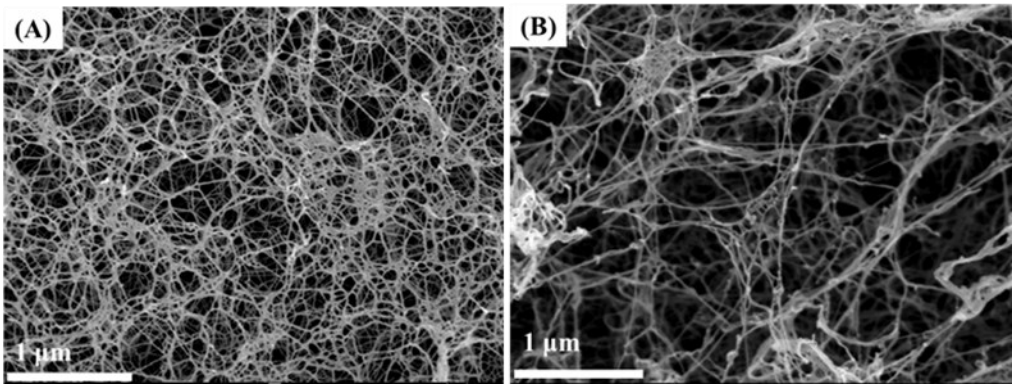


Fig. 1. FE-SEM images of TOCNF (A) and ChNF (B)

Formation and Stability of TOCNF/ChNF Hydrogels

Effect of hydrothermal temperature

Figure 2A shows the digital photographs of hydrogels prepared at a concentration of 1.50 wt% and hydrothermally treated for 2 h at different temperatures. Pure TOCNF hydrogels produced at 110 and 130 °C lost their cylindrical shape upon removal from water, whereas TOCNF/ChNF hydrogels retained their structural integrity. This stability is attributed to enhanced interactions and network formation between TOCNF and ChNF. At 150 °C, the hydrogels developed a noticeable brown coloration, which was likely due to partial carbonization at elevated temperatures. Based on these observations, 130 °C was chosen as the optimal condition for subsequent experiments.

Figure 2B presents the viscosity profiles of TOCNF and TOCNF/ChNF hydrogels prepared at different temperatures, as a function of shear rate. All samples exhibited typical shear-thinning behavior, with viscosity decreasing as shear rate increased. This observation is in line with expectations (Besbes *et al.* 2011). There was not much difference in viscosity observed according to treatment temperature. However, TOCNF/ChNF hydrogels showed higher viscosity than pure TOCNF hydrogels. This enhancement is attributed to enhanced interactions between TOCNF and ChNF, which contribute to improved network formation (Moberg *et al.* 2017; Mendoza *et al.* 2018).

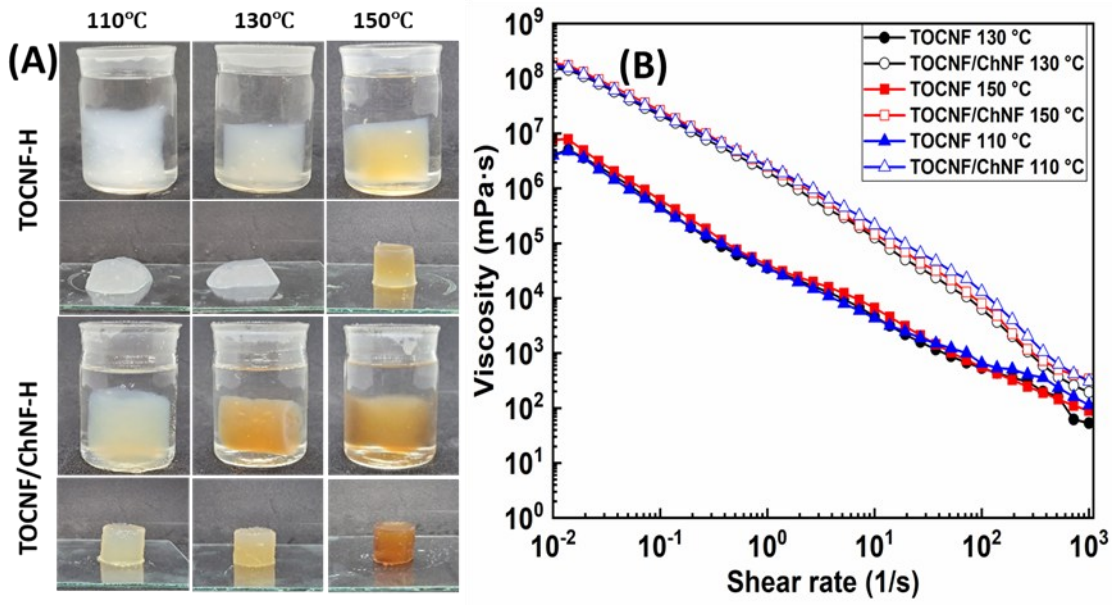


Fig. 2. (A) Photographs of TOCNF and TOCNF/ChNF hydrogels prepared at different temperatures, **(B)** Steady-state viscosity as a function of shear rate for TOCNF and TOCNF/ChNF hydrogels prepared at 110 °C, 130 °C, and 150 °C. (Note: Suspension concentration = 1.50 wt%; reaction time = 2 h)

Effect of suspension concentration

Figure 3A shows digital photographs of TOCNF and TOCNF/ChNF hydrogels prepared at different suspension concentrations and treated at 130 °C for 2 h. All hydrogels retained their shape, except for pure TOCNF at 1.25 and 1.50 wt%, which collapsed upon removal from water, indicating insufficient network integrity at lower concentrations. Figure 3B presents the shear viscosity profiles of TOCNF, TOCNF-H, TOCNF/ChNF, and TOCNF/ChNF-H hydrogels at various concentrations. In all cases, viscosity decreased with increasing shear rate, confirming typical shear-thinning behavior. For TOCNF, hydrothermal treatment resulted in a slight decrease in viscosity at each concentration, suggesting partial disruption or rearrangement of the fibrillar network. In contrast, TOCNF/ChNF hydrogels showed no significant change in viscosity upon treatment. Notably, TOCNF/ChNF hydrogels consistently exhibited higher viscosity than TOCNF alone across all concentrations. This behavior indicates the formation of a more interconnected and entangled fibrillar network in the presence of ChNF, which requires greater energy to deform under shear. These results demonstrate that suspension concentration and ChNF incorporation collectively influence the network structure and rheological behavior of the hydrogels.

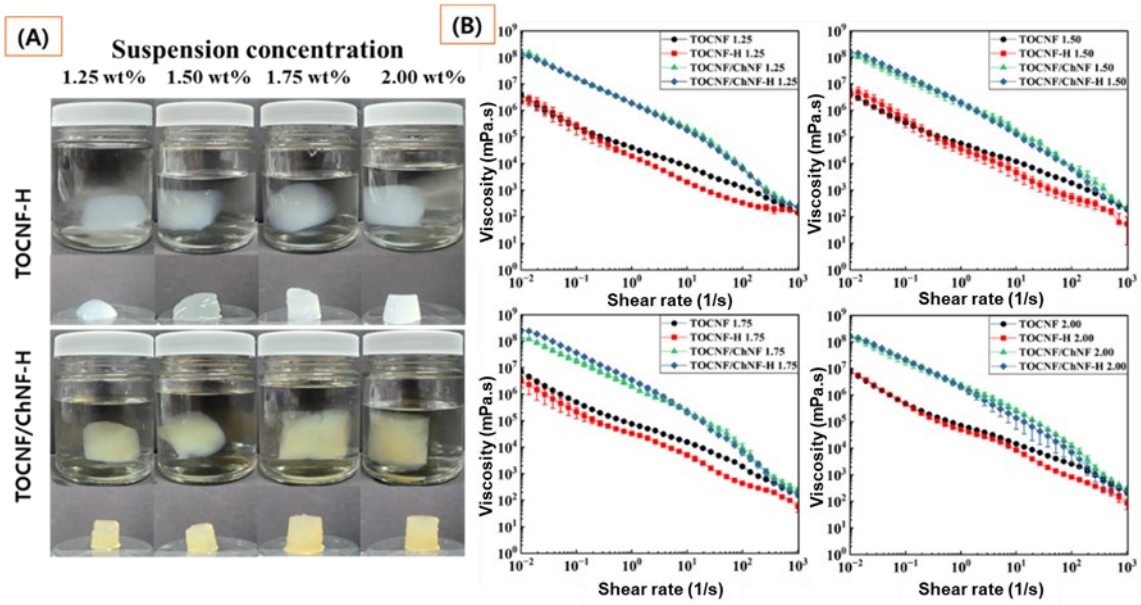


Fig. 3. (A) Photographs of TOCNF and TOCNF/ChNF hydrogels prepared by hydrothermal treatment at different suspension concentrations, **(B)** Steady-state viscosity as a function of shear rate for TOCNF, TOCNF-H, TOCNF/ChNF, and TOCNF/ChNF-H hydrogels prepared at 1.25, 1.50, 1.75, and 2.00 wt% suspension concentrations (Note: Hydrothermal treatment at 130 °C for 2 h)

Rheological Properties

Figure 4A shows the storage modulus (G′) and loss modulus (G″) of TOCNF, TOCNF-H, TOCNF/ChNF, and TOCNF/ChNF-H hydrogels as a function of shear strain. In all cases, *G′* exceeded *G″* within the linear viscoelastic region (up to 10% strain), indicating dominant elastic behavior (Jannatamani *et al.* 2022). The incorporation of ChNF increased both moduli, and further enhancement was observed upon hydrothermal treatment. In contrast, hydrothermal treatment of pure TOCNF led to a reduction in both *G′* and *G″*, suggesting network destabilization (Jannatamani *et al.* 2022). Figure 4B presents the corresponding tan δ (*G″*/*G′*) values, which provide insight into viscoelastic behavior. A tan $\delta < 1$ denotes solid-like characteristics with elastic dominance, tan $\delta = 1$ marks the transition point between solid- and liquid-like states, and tan $\delta > 1$ indicates viscous dominance (Issa *et al.* 2025). The TOCNF hydrogel showed a gradual increase in tan δ with strain, reaching the transition point at 53.3% strain. For the TOCNF-H sample, the transition occurred earlier at 43.9% strain, consistent with weakened network stability upon heating. The TOCNF/ChNF hydrogel exhibited the highest tan δ values, with the transition occurring at 26.3% strain, suggesting that electrostatic interactions between TOCNF and ChNF are readily disrupted under deformation. In contrast, the TOCNF/ChNF-H hydrogel maintained the lowest tan δ values and reached the transition point only at 74.6% strain, reflecting strong intermolecular interactions and improved network integrity. The significant shift in the tan δ transition from 26.3% strain for TOCNF/ChNF to 74.6% strain after hydrothermal treatment indicates a substantial enhancement in network stability. This behavior suggests that, while ChNF contributed to network formation, hydrothermal treatment was the primary factor governing the improved resistance to deformation and structural integrity of the hydrogel system.

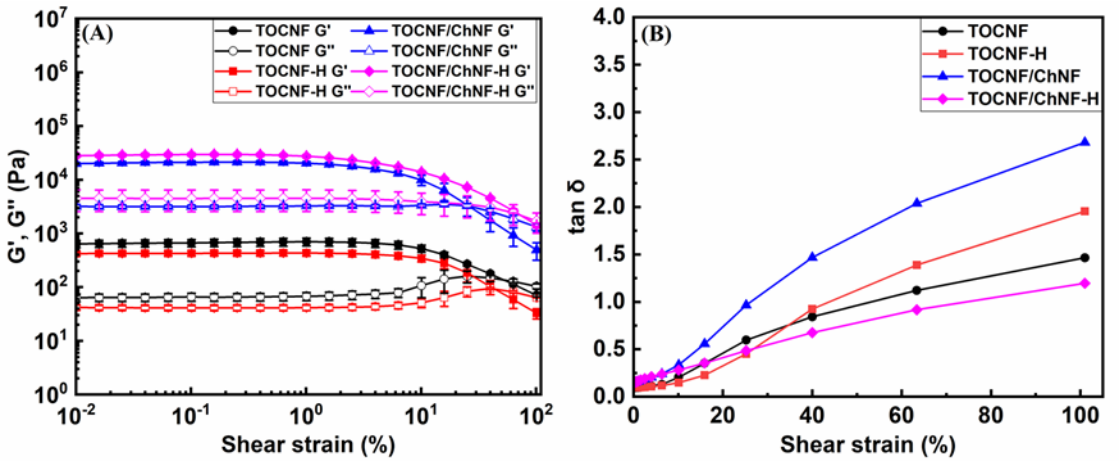


Fig. 4. (A) Storage modulus (*G'*), loss modulus (*G"*) and **(B)** tan *δ* as a function of shear strain of hydrogels (Note: Suspension concentration = 1.75 wt%; Hydrothermal treatment at 130 °C for 2 h)

Mechanical Properties of Hydrogels

Figure 5 presents the compressive stress–strain curves of TOCNF/ChNF-H hydrogels prepared at various concentrations and subjected to hydrothermal treatment at 130 °C. The compressive strength increased with increasing solid content, reaching 22 kPa at 1.25 wt%, 29 kPa at 1.50 wt%, and a maximum of 36 kPa at 1.75 wt%. A slight decrease to 35 kPa was observed at 2.00 wt%, which may be attributed to structural densification or reduced deformability at higher concentrations. In sharp contrast, TOCNF-H hydrogels prepared without ChNF reinforcement exhibited remarkably lower compressive strengths of only ~5 kPa, even at higher concentrations (1.50 to 2.00 wt%). This striking difference underscores the crucial role of ChNF incorporation and subsequent hydrothermal treatment in reinforcing the hydrogel network and enhancing its load-bearing capacity. Notably, the compressive strength values of the present TOCNF/ChNF hydrogels greatly surpassed those of previously reported carboxymethyl cellulose nanofibril/ChNF hydrogels crosslinked with citric acid, which exhibited strengths below 8 kPa (Jung *et al.* 2023).

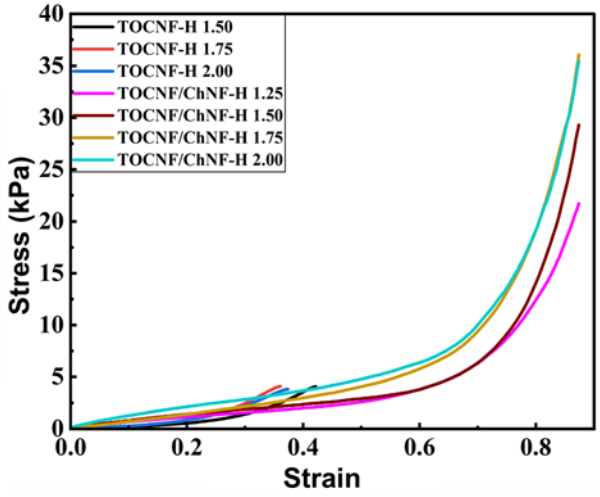


Fig. 5. Stress-strain curve of TOCNF-H and TOCNF/ChNF-H hydrogels prepared at different suspension concentrations (Note: Hydrothermal treatment at 130 °C for 2 h)

It is important to note that TOCNF/ChNF hydrogels without hydrothermal treatment did not exhibit sufficient structural integrity to maintain a stable shape during handling, and thus could not be subjected to compressive testing. This observation indicates that, although ChNF incorporation enhanced initial network formation through electrostatic and hydrogen bonding interactions, these interactions alone were insufficient to provide adequate mechanical stability. The results suggest that hydrothermal treatment plays a critical role in reinforcing the fibrillar network and enabling the development of mechanically robust hydrogels. The improved compressive strength and structural stability of the TOCNF/ChNF hydrogels suggest their potential suitability for applications requiring mechanically robust biopolymer networks, such as adsorbent materials, structural supports, and stable hydrogel matrices (Tamo 2024) (Zhang *et al.* 2019).

FTIR Analysis

To investigate the interactions between TOCNF and ChNF, the FTIR spectra of lyophilized TOCNF, ChNF, TOCNF/ChNF, and TOCNF/ChNF-H samples were recorded (Fig. 6). The spectrum of ChNF exhibits characteristic absorption bands associated with chitin, including the amide I doublet at approximately 1651 and 1620 cm^{-1} and the amide II band at 1556 cm^{-1}, which originate from the C=O stretching and N–H bending vibrations of the amide groups, respectively. Additional fingerprint peaks corresponding to C–O stretching (1310 cm^{-1}) and out-of-plane –OH bending (951 cm^{-1}) were also observed (Zhang *et al.* 2019). In contrast, the TOCNF spectrum shows a prominent band at approximately 1600 cm^{-1}, corresponding to the asymmetric stretching vibration of the carboxylate ($–COO^-$) groups introduced during TEMPO oxidation. A symmetric $–COO^-$ stretching band is also apparent at 1369 cm^{-1} (da Silva Perez *et al.* 2003). The FTIR spectrum of the TOCNF/ChNF hydrogel displays characteristic features of both TOCNF and ChNF. However, the bands associated with the carboxylate groups of TOCNF and the amide groups of ChNF partially overlap, resulting in a broad absorption band in the 1700 to 1500 cm^{-1} region. This behavior suggests strong interactions between the negatively charged carboxylate groups of TOCNF and the amino groups present on the ChNF surface, which likely contribute to the formation of the hydrogel network through electrostatic attraction and hydrogen bonding. After hydrothermal treatment, the TOCNF/ChNF-H sample shows subtle changes in the spectral region between 1700 and 1500 cm^{-1}, where the overlapping bands become slightly more distinguishable. These spectral changes indicate that hydrothermal treatment altered the interactions between TOCNF and ChNF within the hydrogel network. Although such changes may be consistent with possible condensation reactions between carboxyl and amino groups, the FTIR data alone do not provide definitive evidence for covalent bond formation. Instead, the results suggest that hydrothermal treatment modifies the intermolecular interactions and structural organization within the fibrillar network.

To further examine hydrogen-bonding interactions, the FTIR spectra in the 3700 to 3000 cm^{-1} region were separately analyzed in absorbance mode using baseline correction followed by Gaussian peak deconvolution (Fig. S1). The corresponding peak positions and relative peak areas are summarized in Tables S1a and S1b. The broad O–H/N–H stretching region could be deconvoluted into five characteristic components associated with hydrogen-bonding environments in cellulose and chitin systems. For cellulose, the bands centered at approximately 3549 and 3438 cm^{-1} were assigned to intramolecular O(2)H···O(6) and O(3)H···O(5) hydrogen bonds, respectively, while the band at 3332 cm^{-1} corresponds to intermolecular O(6)H···O(3′) hydrogen bonding (Feng *et al.* 2018). In the

chitin component, the peak at ~3130 cm^{-1} is attributed to intermolecular O(6)H···O(6′) hydrogen bonding, whereas the peak at ~3242 cm^{-1} is assigned to intermolecular C(2)NH···O(6′) interactions involving amino groups of chitin chains (Feng *et al.* 2018).

After hydrothermal treatment, the TOCNF/ChNF-H sample exhibited similar peak distributions with slight changes in peak positions and relative peak areas compared with TOCNF/ChNF. In particular, the relative area of the ~3438 cm^{-1} band increased from 17.1% to 19.8%, while the contribution of the ~3242 cm^{-1} band decreased slightly from 24.1% to 22.0%. These subtle changes indicate redistribution of hydrogen-bonding interactions (Song *et al.* 2022) and enhanced interfibrillar interactions within the hydrogel network after hydrothermal treatment. However, no substantial peak shifts or new absorption bands were observed, further supporting that hydrothermal treatment primarily promotes structural rearrangement and strengthening of intermolecular interactions rather than significant new covalent bond formation (Suenaga *et al.* 2019).

XPS Analysis

X-ray photoelectron spectroscopy (XPS) was employed to further analyze the surface chemical composition of the samples. The survey spectrum of TOCNF showed two characteristic peaks at 285 eV (C 1s) and 530 eV (O 1s) (Fig. 6B). In the case of ChNF, an additional N 1s peak at approximately 400 eV was observed, reflecting the presence of nitrogen-containing functional groups associated with the partially deacetylated chitin structure. The N 1s signal was also detected in both the TOCNF/ChNF and TOCNF/ChNF-H samples, confirming the successful incorporation of ChNF within the TOCNF-based hydrogel network. High-resolution analysis of the N 1s region (Fig. 6C) revealed a slight shift toward higher binding energy after hydrothermal treatment. Such a shift suggests a change in the chemical environment of nitrogen atoms, which may arise from stronger interactions between the amino groups of ChNF and the carboxyl groups of TOCNF. The presence of an electron-withdrawing carbonyl environment can increase the binding energy of nitrogen species, and therefore this shift may be consistent with the formation of new interfacial interactions during hydrothermal treatment (He *et al.* 2017). However, as the shift was relatively small and other nitrogen-containing species may contribute to the signal, the XPS data should be interpreted cautiously and do not provide definitive evidence for covalent amide bond formation.

To further examine these interactions, the high-resolution C 1s spectra of TOCNF/ChNF and TOCNF/ChNF-H were deconvoluted (Fig. S2). The spectra were fitted into four components: C1 (C–C/C–H), C2 (C–O/C–N), C3 (C–O–C/C=O), and C4 (O–C=O) (Zhang *et al.* 2019). The corresponding peak positions and relative peak areas are summarized in Tables S2a and S2b. Only minor shifts in peak positions were observed after hydrothermal treatment, indicating no significant change in chemical bonding states. In terms of peak area distribution, the relative contribution of the C1 component increased from 19.6% to 22.6%, while the contributions of C2, C3, and C4 decreased slightly.

This redistribution suggests structural reorganization and partial densification of the fibrillar network rather than the formation of new covalent bonds. The increase in the C1 fraction, together with the reduction in oxygen-containing components, may reflect closer packing and enhanced interfibrillar interactions within the hydrogel network after hydrothermal treatment.

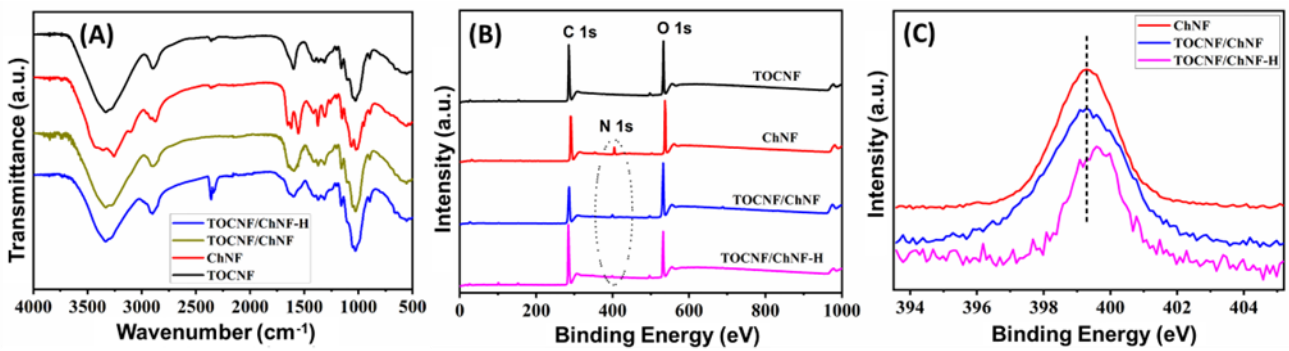


Fig. 6. FT-IR spectra **(A)**, XPS survey scans **(B),** and high-resolution N 1s scans **(C)** for TOCNF, ChNF, TOCNF/ChNF, and TOCNF/ChNF-H (Note: Suspension concentration = 1.75 wt%; Hydrothermal treatment at 130 °C for 2 h)

Hydrogel Morphology

SEM images of the TOCNF/ChNF and hydrothermally treated TOCNF/ChNF (TOCNF/ChNF-H) hydrogels are presented in Fig. 7. The TOCNF/ChNF hydrogels prepared by simple mixing exhibited a disordered and heterogeneous porous structure with irregular pore distribution and loosely connected fibrillar walls (Fig. 7A&B). In contrast, the TOCNF/ChNF-H hydrogels displayed a more uniform and interconnected porous network with a honeycomb-like morphology and thicker pore walls (Fig. 7C&D). Such structural refinement suggests network densification and improved interfibrillar connectivity after hydrothermal treatment, which is known to enhance mechanical performance in nanocellulose-based systems (De France *et al*. 2017; Sehaqui *et al.* 2011). Similar interconnected structures have been reported in nanocellulose–chitin hybrid systems, where improved network organization contributes to enhanced structural stability (Zhang *et al.* 2019). The observed morphological evolution is consistent with improved load distribution and mechanical strength, as supported by previous studies correlating pore structure and network connectivity with rheological and mechanical properties (Mendoza *et al.* 2018).

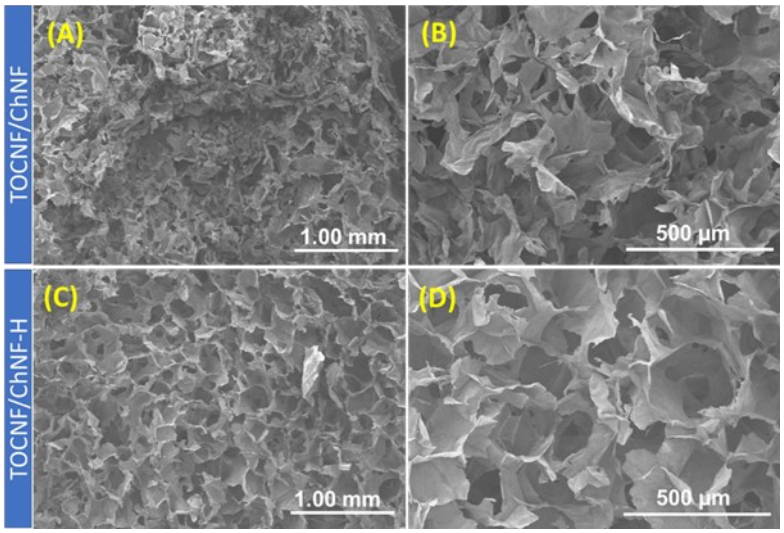


Fig. 7. FE-SEM images of TOCNF/ChNF **(A&B)**, and TOCNF/ChNF-H **(C&D)** hydrogels at low **(A&C)** and high **(B&D)** magnifications (Note: Suspension concentration = 1.75 wt%; Hydrothermal treatment at 130 °C for 2 h)

Thermal Properties

TGA curves of TOCNF, ChNF, TOCNF/ChNF, and TOCNF/ChNF-H are presented in Fig. S3, with detailed analysis provided in the Supporting Information. The results show that the incorporation of ChNF improved the thermal stability of the composites compared to TOCNF alone. However, no significant difference was observed between the physically crosslinked and hydrothermally treated samples, indicating that hydrothermal treatment had a limited effect on thermal stability relative to the intrinsic properties of the constituent polymers.

Limitations

Although the TOCNF/ChNF hydrogels showed improved structural stability and mechanical performance after hydrothermal treatment, several limitations should be noted. First, the non-treated TOCNF/ChNF hydrogels did not possess sufficient shape stability for reliable compressive testing, which limited direct comparison between the effects of ChNF incorporation and hydrothermal treatment. Second, while FTIR and XPS analyses indicated changes in intermolecular interactions after hydrothermal treatment, the available spectroscopic evidence was insufficient to conclusively identify the exact strengthening mechanism or confirm covalent bond formation. Third, hydrothermal treatment at elevated temperatures caused visible browning of the hydrogels, indicating the possibility of undesired thermal degradation under harsh treatment conditions. Therefore, careful control of hydrothermal treatment conditions is necessary to balance structural stability and preservation of material properties.

CONCLUSIONS

1. TEMPO-oxidized cellulose nanofibril/chitosan nanofibril (TOCNF/ChNF) hydrogels were successfully prepared, and ChNF incorporation was found to improve structural stability, enabling well-defined gel formation at low solid contents.
2. Hydrothermal treatment played a critical role in reinforcing the fibrillar network, resulting in enhanced hydrogel integrity and mechanical stability.
3. TOCNF/ChNF hydrogels exhibited higher viscosity and pronounced shear-thinning behavior compared to TOCNF alone, indicating a more entangled fibrillar network.
4. Hydrothermally treated TOCNF/ChNF hydrogels maintained elastic behavior over a wider strain range, demonstrating improved resistance to deformation and network stability.
5. Compressive strength increased greatly with ChNF incorporation and gel concentration, reaching 36 kPa at 1.75 wt%, compared to ~5 kPa for TOCNF hydrogels.
6. The Fourier transform infrared (FTIR), XPS, and SEM indicated that ChNF incorporation and hydrothermal treatment modified intermolecular interactions, promoted network densification.

ACKNOWLEDGMENTS

This research was supported by the National Institute of Forest Science and Basic Science Research Program through the National Research Foundation of Korea (NRF) funded by the Ministry of Education (No. RS-2018-NR031068 and No. RS-2021-NR059094).

Conflict of Interest

The authors declare that they have no conflict of interest.

Use of Generative AI

During the preparation of manuscript, the author(s) used [ChatGPT] in order to improve the readability and language. After using this tool/service, the author(s) reviewed and edited the content as needed and take(s) full responsibility for the content of the publication.

REFERENCES CITED

Ahmed, E. M. (2015). "Hydrogel: Preparation, characterization, and applications: A review," *Journal of Advanced Research* 6(2), 105-121. https://doi.org/10.1016/J.JARE.2013.07.006

Alghonaim, M. I., Alsalamah, S. A., Bazaid, A. S., and Abdelghany, T. M. (2024). "Biosynthesis of CuO@Au NPs and its formulated into biopolymers carboxymethyl cellulose and chitosan: Characterizations, antimicrobial, anticancer and antioxidant properties," *Waste and Biomass Valorization* 15(9), 5191-5204. https://doi.org/10.1007/s12649-024-02469-5

Altynov, Y., Bexeitova, K., Nazhipkyzy, M., Azat, S., Konarov, A., Rakhman, D., Sahiner, N., and Kudaibergenov, K. (2025). "Nanocellulose hydrogels from agricultural wastes: Methods, properties, and application prospects," *Nanoscale* 17(20), 12580-12619. https://doi.org/10.1039/D5NR00997A

Besbes, I., Alila, S., and Boufi, S. (2011). "Nanofibrillated cellulose from TEMPO-oxidized eucalyptus fibres: Effect of the carboxyl content," *Carbohydrate Polymers* 84(3), 975-983. https://doi.org/10.1016/J.CARBPOL.2010.12.052

Chinga-Carrasco, G. (2018). "Potential and limitations of nanocelluloses as components in biocomposite inks for three-dimensional bioprinting and for biomedical devices," *Biomacromolecules* 19(3), 701-711. https://doi.org/10.1021/ACS.BIOMAC.8B00053

Correa, S., Grosskopf, A. K., Lopez Hernandez, H., Chan, D., Yu, A. C., Stapleton, L. M., and Appel, E. A. (2021). "Translational applications of hydrogels," *Chemical Reviews* 121(18), 11385-11457. https://doi.org/10.1021/ACS.CHEMREV.0C01177

Du, Y., and Feng, G. (2023). "When nanocellulose meets hydrogels: The exciting story of nanocellulose hydrogels taking flight," *Green Chemistry* 25(21), 8349-8384. https://doi.org/10.1039/D3GC01829F

De France, K. J., Hoare, T., and Cranston, E. D. (2017). "Review of hydrogels and aerogels containing nanocellulose," *Chemistry of Materials* 29(11), 4609-4631. https://doi.org/10.1021/acs.chemmater.7b00531

Feng, Y., Li, J., Wang, B., Tian, X., Chen, K., Zeng, J., Xu, J., and Gao, W. (2018). "Novel nanofibrillated cellulose/chitin whisker hybrid nanocomposites and their use

for mechanical performance enhancements" *BioResources* 13(2), 3030-3044. https://doi.org/10.15376/biores.13.2.3030-3044

He, H., Hu, Y., Chen, S., Zhuang, L., Ma, B., and Wu, Q. (2017). "Preparation and properties of a hyperbranch-structured polyamine adsorbent for carbon dioxide capture," *Scientific Reports* 7(1), article 3913. https://doi.org/10.1038/s41598-017-04329-w

Issa, M. C. A., Viana, R. M. M., de Souza Mendes, P. R., Naccache, M. F., Varges, P. R., Castaño, E. P. M., and Palermo, E. (2025). "Analysis of morphologic and rheological properties of hyaluronic acid gel fillers to body contouring and its clinical correlation," *Gels* 11(1), article 65. https://doi.org/10.3390/GELS11010065

Jannatamani, H., Motamedzadegan, A., Farsi, M., and Yousefi, H. (2022). "Rheological properties of wood/bacterial cellulose and chitin nano-hydrogels as a function of concentration and their nano-films properties," *IET Nanobiotechnology* 16(4), 158-169. https://doi.org/10.1049/NBT2.12083

Jin, S. A., and Spontak, R. J. (2023). "Fundamentals of and advances in nanocellulose and nanochitin systems," *Advanced Industrial and Engineering Polymer Research* 6(4), 356-381. https://doi.org/10.1016/J.AIEPR.2023.04.003

Jin, T., Liu, T., Lam, E., and Moores, A. (2021). "Chitin and chitosan on the nanoscale," *Nanoscale Horizons* 6(7), 505-542. https://doi.org/10.1039/d0nh00696c

Jung, S., Kim, J., Bang, J., Jung, M., Park, S., Yun, H., and Kwak, H. W. (2023). "pH-sensitive cellulose/chitin nanofibrillar hydrogel for dye pollutant removal," *Carbohydrate Polymers* 317, article 121090. https://doi.org/10.1016/J.CARBPOL.2023.121090

Lan, X., Ma, Z., Szojka, A. R. A., Kunze, M., Mulet-Sierra, A., Vyhlidal, M. J., Boluk, Y., and Adesida, A. B. (2021). "TEMPO-oxidized cellulose nanofiber-alginate hydrogel as a bioink for human meniscus tissue engineering," *Frontiers in Bioengineering and Biotechnology* 9, article 766399. https://doi.org/10.3389/fbioe.2021.766399

Liang, L., Bhagia, S., Li, M., Huang, C., and Ragauskas, A. J. (2020). "Cross-linked nanocellulosic materials and their applications," *ChemSusChem* 13(1), 78-87. https://doi.org/10.1002/CSSC.201901676

Mehvari, F., Ramezanzade, V., An, J., Kim, J., Dinari, M., and Seung Kim, J. (2024). "Biopolymer-based hydrogels for biomedical applications: Bioactivity and wound healing properties," *Coordination Chemistry Reviews* 518, article 216093. https://doi.org/10.1016/j.ccr.2024.216093

Mendoza, L., Batchelor, W., Tabor, R. F., and Garnier, G. (2018). "Gelation mechanism of cellulose nanofibre gels: A colloids and interfacial perspective," *Journal of Colloid and Interface Science* 509, 39-46. https://doi.org/10.1016/J.JCIS.2017.08.101

Moberg, T., Sahlin, K., Yao, K., Geng, S., Westman, G., Zhou, Q., Oksman, K., and Rigdahl, M. (2017). "Rheological properties of nanocellulose suspensions: Effects of fibril/particle dimensions and surface characteristics," *Cellulose* 24(6), 2499-2510. https://doi.org/10.1007/s10570-017-1283-0

Nata, I. F., Wang, S. S. S., Wu, T. M., and Lee, C. K. (2012). "β-Chitin nanofibrils for self-sustaining hydrogels preparation via hydrothermal treatment," *Carbohydrate Polymers* 90(4), 1509-1514. https://doi.org/10.1016/j.carbpol.2012.07.022

Nikolits, I., Radwan, S., Liebner, F., Dietrich, W., Egger, D., Chariyev-Prinz, F., and Kasper, C. (2023). "Hydrogels from TEMPO-oxidized nanofibrillated cellulose

support *in vitro* cultivation of encapsulated human mesenchymal stem cells," *ACS Applied Bio Materials* 6(2), 543-551. https://doi.org/10.1021/ACSABM.2C00854

Noda, T., Hatakeyama, M., and Kitaoka, T. (2022). "Combination of polysaccharide nanofibers derived from cellulose and chitin promotes the adhesion, migration and proliferation of mouse fibroblast cells," *Nanomaterials* 12(3), article 402. https://doi.org/10.3390/NANO12030402/S1

Saied, M., Hasanin, M., Abdelghany, T. M., Amin, B. H., and Hashem, A. H. (2013). "Anticandidal activity of nanocomposite based on nanochitosan, nanostarch and mycosynthesized copper oxide nanoparticles against multidrug-resistant *Candida*," *International Journal of Biological Macromolecules* 242, article 124709. https://doi.org/10.1016/j.ijbiomac.2023.124709

Sehaqui, H., Zhou, Q., and Berglund, L. A. (2011). "High-porosity aerogels of high specific surface area prepared from nanofibrillated cellulose (NFC)," *Composites Science and Technology*, 71(13), 1593-1599.

Sharma, S., Bhende, M., and Goel, A. (2024). "A review: Polysaccharide-based hydrogels and their biomedical applications," *Polymer Bulletin* 81(10), 8573-8594. https://doi.org/10.1007/s00289-023-05130-8

Shen, X., Shamshina, J. L., Berton, P., Gurau, G., and Rogers, R. D. (2015). "Hydrogels based on cellulose and chitin: Fabrication, properties, and applications," *Green Chemistry* 18(1), 53-75. https://doi.org/10.1039/c5gc02396c

Shi, M., Liang, Y., Zhang, C., Li, N., Li, Y., Shi, X., Qin, Z., and Jiao, T. (2025). "Cellulose nanofibril enhanced ionic conductive hydrogels with high stretchability, high toughness and self-adhesive ability for flexible strain sensors," *International Journal of Biological Macromolecules* 293, article 139297. https://doi.org/10.1016/J.IJBIOMAC.2024.139297

da Silva Perez, D., Montanari, S., and Vignon, M. R. (2003). "TEMPO-Mediated oxidation of cellulose III," *Biomacromolecules* 4(5), 1417-1425. https://doi.org/10.1021/BM034144S

Song, H., Yang, J., Yang, Y., Yang, Q., and Hu, J. (2022). "Characterization of cellulose-nanofiber-modified fibrillated lyocell fiber separator," *BioResources* 17(3), 4689-4706. https://doi.org/10.15376/biores.17.3.4689-4704

Suenaga, S., and Osada, M. (2018). "Self-sustaining cellulose nanofiber hydrogel produced by hydrothermal gelation without additives," *ACS Biomaterials Science & Engineering* 4(5), 1536-1545. https://doi.org/10.1021/acsbiomaterials.8b00026

Suenaga, S., and Osada, M. (2019). "Hydrothermal gelation of pure cellulose nanofiber dispersions," *ACS Applied Polymer Materials* 1(5), 1045-1053. https://doi.org/10.1021/acsapm.9b00076

Tamo, A. K. (2024). "Nanocellulose-based hydrogels as versatile materials with interesting functional properties for tissue engineering applications," *Journal of Materials Chemistry B* 12(32), 7692-7759. https://doi.org/10.1039/D4TB00397G

Tang, Z., Lin, X., Yu, M., Mondal, A. K., and Wu, H. (2024). "Recent advances in TEMPO-oxidized cellulose nanofibers: Oxidation mechanism, characterization, properties and applications," *International Journal of Biological Macromolecules* 259, article 129081. https://doi.org/10.1016/J.IJBIOMAC.2023.129081

Tariq, Z., Iqbal, D. N., Rizwan, M., Ahmad, M., Faheem, M., and Ahmed, M. (2023). "Significance of biopolymer-based hydrogels and their applications in agriculture: A review in perspective of synthesis and their degree of swelling for water holding," *RSC Advances* 13(35), 24731-24754. https://doi.org/10.1039/d3ra03472k

Tsutsumi, Y., Koga, H., Qi, Z.-D., Saito, T., and Isogai, A. (2014). "Nanofibrillar chitin aerogels as renewable base catalysts," *Biomacromolecules* 15(11), 4314-4319. https://doi.org/10.1021/bm501320b

Wasupalli, G. K., and Verma, D. (2023). "Development of chitosan-polygalacturonic acid polyelectrolyte complex fibrous scaffolds using the hydrothermal treatment for bone tissue engineering," *Journal of Biomedical Materials Research Part A*, 111(3), 354-366. https://doi.org/10.1002/jbm.a.37461

Zafar, S., Hanif, M., Azeem, M., Mahmood, K., and Gondal, S. A. (2022). "Role of crosslinkers for synthesizing biocompatible, biodegradable and mechanically strong hydrogels with desired release profile," *Polymer Bulletin* 79(11), 9199-9219. https://doi.org/10.1007/s00289-021-03956-8

Zhang, X., Elsayed, I., Navarathna, C., Schueneman, G. T., and Hassan, E. B. (2019). "Biohybrid hydrogel and aerogel from self-assembled nanocellulose and nanochitin as a high-efficiency adsorbent for water purification," *ACS Applied Materials & Interfaces* 11(50), 46714-46725. https://doi.org/10.1021/acsami.9b15139

Article submitted: March 26, 2026; Peer review completed: April 14, 2026; Revised version received and accepted: May 6, 2026; Published: May 18, 2026.
DOI: 10.15376/biores.21.3.6016-6035

APPENDIX

Determination of Amine and Carboxyl Group Contents

The primary amine (−NH_2) content of ChNF was determined by conductometric titration. Briefly, a dispersion containing 70 mg of ChNF in 60 mL of 1.5 mM NaCl solution was prepared under magnetic stirring. The pH of the dispersion was adjusted to 3 using 0.1 M HCl to ensure protonation of amine groups. Titration was then performed by adding 100 mM NaOH solution at a constant rate of 0.1 mL·min^{-1} while monitoring conductivity. The amine content was calculated from the conductivity versus titrant volume curve using the following equation:

$$\text{Amine content (mmol/g)} = C_{NaOH} \times (V_2 - V_1)/m$$

where C_{NaOH} is the concentration of NaOH (mM), V_1 and V_2 are the equivalence points (mL) determined from the titration curve, and m is the mass of the ChNF sample (mg).

The carboxyl group content of TOCNF sample was also determined by conductometric titration. A 50 mL suspension (0.1 wt%) was first acidified by adding 1 mL of 0.1 M HCl and stirred for 30 min to protonate the carboxyl groups. The sample was then titrated with 0.02 M NaOH solution under continuous stirring. The carboxyl content was calculated from the conductivity–volume curve using the following equation:

$$\text{Carboxyl content (mmol/g)} = C_{NaOH} \times (V_2 - V_1)/m$$

where C_{NaOH} is the concentration of NaOH (mM), V_1 and V_2 are the equivalence volumes (mL), and m is the mass of the dry sample (mg).

The carboxyl group content of TOCNF was determined to be 0.69 ± 0.03 mmol/g, while the primary amine content of ChNF was measured as 3.43 ± 0.04 mmol/g.

FTIR analysis

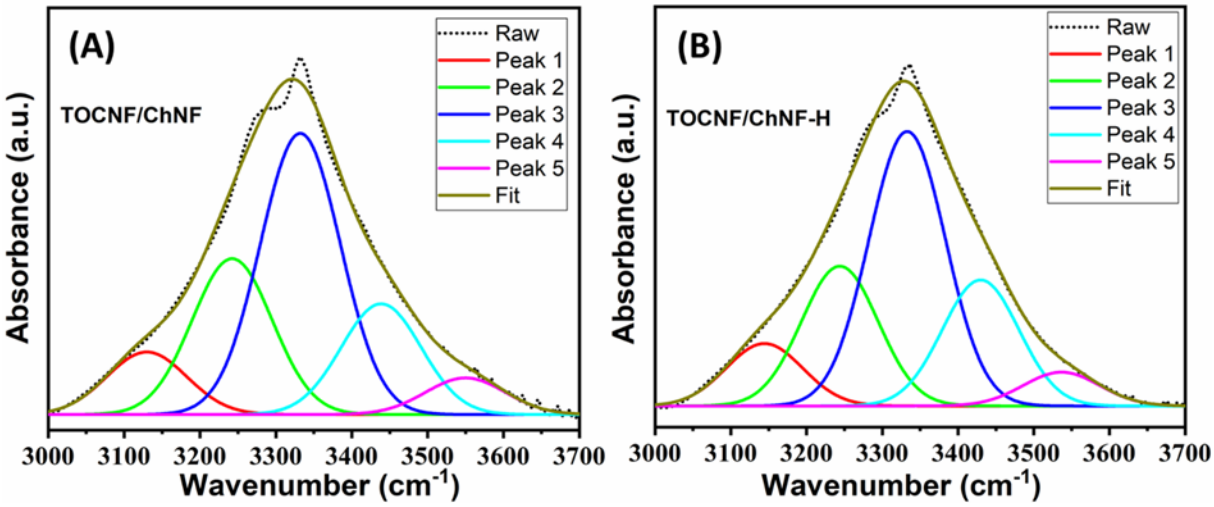


Fig. S1. Gaussian peak deconvolution of the FTIR O–H/N–H stretching region (3700 to 3000 cm^{-1}) for TOCNF/ChNF (A) and TOCNF/ChNF-H (B)

Table S1a. Peak Positions Obtained from Gaussian Deconvolution of the FTIR O–H/N–H Stretching Region (3700 to 3000 cm^{-1})

	Peak 1 (cm^{-1})	Peak 2 (cm^{-1})	Peak 3 (cm^{-1})	Peak 4 (cm^{-1})	Peak 5 (cm^{-1})
TOCNF/ChNF	3130	3242	3332	3438	3549
TOCNF/ChNF-H	3144	3243	3332	3429	3536

Table S1b. Relative Peak Areas (%) Obtained from Gaussian Deconvolution of the FTIR O–H/N–H Stretching Region (3700 to 3000 cm^{-1})

	Peak 1(%)	Peak 2(%)	Peak 3(%)	Peak 4(%)	Peak 5(%)
TOCNF/ChNF	9.66	24.09	43.48	17.11	5.65
TOCNF/ChNF-H	9.80	21.96	43.14	19.79	5.29

XPS Analysis

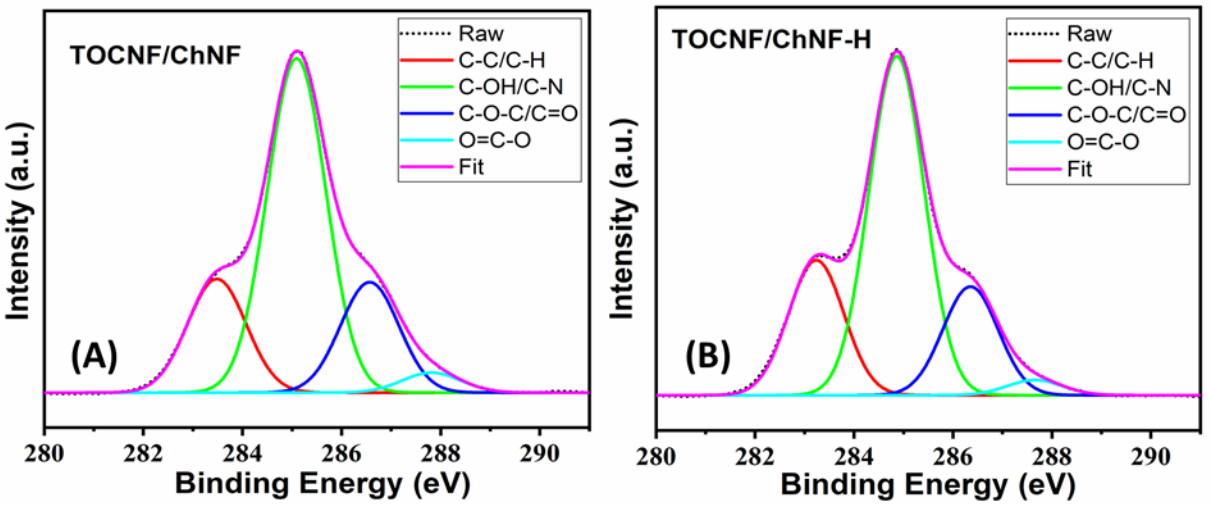


Fig. S2. High-resolution XPS C 1s spectra and peak deconvolution of TOCNF/ChNF (A) and TOCNF/ChNF-H (B)

Table S2a. Relative Peak Area Distribution (%) of Deconvoluted C 1s Components Obtained from XPS Analysis

	C1(%)	C2(%)	C3(%)	C4(%)
TOCNF/ChNF	19.65	57.82	19.09	3.44
TOCNF/ChNF-H	22.59	56.72	18.16	2.53

Table S2b. Binding Energies of Deconvoluted C 1s Components Obtained from XPS Analysis

	C1(eV)	C2(eV)	C3(eV)	C4(eV)
TOCNF/ChNF	283.48	285.09	286.56	287.81
TOCNF/ChNF-H	283.23	284.86	286.35	287.65

Thermal Properties

Figure S3 presents the thermogravimetric analysis (TGA) curves of freeze-dried TOCNF, ChNF, TOCNF/ChNF, and TOCNF/ChNF-H samples. All samples exhibited an initial weight loss below 100 °C, corresponding to the evaporation of physically adsorbed moisture.

TOCNF shows a major degradation step in the range of 220 to 320 °C, which is associated with decarboxylation, depolymerization, and cleavage of glycosidic linkages in the cellulose backbone. A secondary degradation region between 330 and 470 °C is attributed to the decomposition of residual crystalline domains (Jiang and Hsieh 2016). In contrast, ChNF exhibits broader thermal degradation behavior, with major weight loss occurring between 264 and 550 °C, corresponding to the decomposition and volatilization of chitin chains (Bombuwala Dewage *et al.* 2018).

The TOCNF/ChNF composite showed a degradation profile spanning the characteristic decomposition regions of both components, indicating the combined thermal behavior of the hybrid system. Quantitatively, the temperature at 50% mass loss (T_{50}%) increased from 309.9 °C for TOCNF to 344.3 °C for TOCNF/ChNF, while ChNF exhibited

a higher value of 375.0 °C. The hydrothermally treated TOCNF/ChNF-H sample showed a comparable T_{50}% value of 345.6 °C.

These results indicate that the incorporation of ChNF improved the thermal stability of the composite, which can be attributed to the higher intrinsic thermal stability of ChNF and enhanced intermolecular interactions within the hybrid network. However, the negligible difference between TOCNF/ChNF and TOCNF/ChNF-H suggests that hydrothermal treatment has a limited effect on thermal stability compared to the compositional contribution of ChNF.

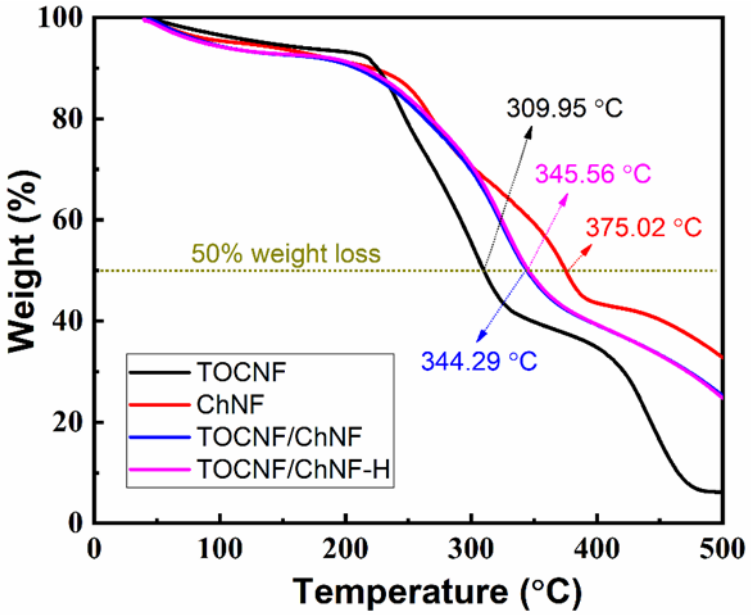


Fig. S3. TGA curves of TOCNF, ChNF, and TOCNF/ChNF and TOCNF/ChNF-H

REFERENCES CITED (APPENDIX)

Bombuwala Dewage, N., Fowler, R. E., Pittman, C. U., Mohan, D., and Mlsna, T. (2018). "Lead (Pb^{2+}) sorptive removal using chitosan-modified biochar: Batch and fixed-bed studies," *RSC Advances* 8(45), 25368-25377. https://doi.org/10.1039/C8RA04600J

Jiang, F., and Hsieh, Y. L. (2016). "Self-assembling of TEMPO oxidized cellulose nanofibrils as affected by protonation of surface carboxyls and drying methods," *ACS Sustainable Chemistry and Engineering* 4(3), 1041-1049. https://doi.org/10.1021/ACSSUSCHEMENG.5B01123